Energy Reports 6 (2020) 2249–2255

Contents lists available at ScienceDirect

Energy Reports

journal homepage: www.elsevier.com/locate/egyr

Research paper

TiO_2-supported Ni-Sn as an effective hydrogenation catalyst for aqueous acetic acid to ethanol

Yuanyuan Zhao, Takayuki Nishida, Eiji Minami, Shiro Saka, Haruo Kawamoto *

Graduate School of Energy Science, Kyoto University, Yoshida-honmachi, Sakyo-ku, Kyoto 606-8501, Japan

ARTICLE INFO

Article history:
Received 25 March 2020
Received in revised form 15 July 2020
Accepted 9 August 2020
Available online xxxx

Keywords:
Bioethanol
Ni-Sn/TiO_2
Hydrogenation
Acetic acid

ABSTRACT

Various Ni and Ni-Sn catalysts supported on TiO_2 were prepared and the catalytic activities were evaluated for ethanol formation from aqueous acetic acid. Although catalytic activities of the Ni/TiO_2 catalysts were limited, the addition of Sn improved the activity dramatically, and the optimum Ni/Sn ratio was approximately 1:1 (w/w). SnO_2, the precursor of Sn, could not be reduced into metal Sn in pure form but did reduce into Ni-Sn alloys in the presence of NiO, the precursor of Ni. Analyses with XRD and SEM-EDS revealed that the Ni-Sn alloys were homogeneously dispersed on the TiO_2 surface. Furthermore, IR analysis indicated that the Ti atoms in the catalyst act as a Lewis acid, which coordinates to the oxygen atoms of acetic acid, enhancing the attack of hydrogens activated on neighboring Ni-Sn alloys. Based on these results, Ni-Sn/TiO_2 is proposed as an effective hydrogenation catalyst for converting aqueous acetic acid into ethanol.

1. Introduction

Fossil fuel shortage has become an urgent problem in the world, especially with regards to oil and natural gas (Pimentel et al., 2008). Biomass resources are used as a substitute for fossil resources in both developed and developing countries, particularly as biofuels (Cleveland et al., 1984; Biello, 2011). Bioethanol receives much attention as one of these biofuel alternatives to gasoline (Osei et al., 2013). Currently, alcohol fermentation predominately uses edible resources, such as sugarcane and starch, as raw materials, causing a risk of increasing food prices (Ajanovic, 2011). In addition, during the alcohol fermentation of hexoses, such as glucose, two carbon atoms are emitted as CO_2, thus decreasing the efficiency of carbon utilization (Rodríguez et al., 2010).

To improve carbon efficiency and avoid food competition, our research group has proposed a highly efficient bioethanol production process via acetic acid fermentation from lignocelluloses, which are non-edible resources (Saka et al., 2019). With acetic acid fermentation, all carbon atoms in glucose can be converted into acetic acid, and thus the carbon efficiency is expected to be improved (Nakamura et al., 2011; Rabemanolontsoa et al., 2016). This new bioethanol production process includes three steps: hot-compressed water treatment to hydrolyze lignocellulose, acetic acid fermentation of resulting hydrolyzates, and hydrogenation of acetic acid into ethanol. The current research is focused on the last step, hydrogenation of acetic acid.

Two different pathways have been reported for the hydrogenation of acetic acid: a two-step reaction via ethyl acetate to ethanol, and direct conversion to ethanol (Adkins and Folkers, 1931; Adkins et al., 1933; Folkers and Adkins, 1932; Rachmady and Vannice, 2000; Voeste and Buchold, 1984). The direct hydrogenation from aqueous acetic acid is desirable for practical use because the two-step reaction via ethyl acetate requires dehydration of acetic acid, which is energetically and economically burdensome (Chien et al., 2004; Lei et al., 2004).

Several papers reported the direct hydrogenation of aqueous acetic acid into ethanol. Elliott and Hart (2009) conducted the catalytic hydrogenation of aqueous acetic acid as a constituent of fast pyrolysis oil over Pd/C and Ru/C under the conditions of 150–300 ° C/ H_2 13.8 MPa/ 0.5–4 h, but the reported yields were only less than 35 mol%. Wan et al. (2013) compared the catalytic activity of various catalysts for hydrogenation of aqueous acetic acid under the conditions of 200 or 300 °C/ H_2 4.8 MPa/ 1 h. They showed that Ru/C exhibited the higher conversion than Ru/Al_2O_3, Pt/C, Pd/C, Pt/Al_2O_3, Pd/C, and Pd/Al_2O_3, but most of the products were methane and ethane. Wang et al. (2014) reported the aqueous acetic acid hydrogenation over Ir-MoO_x/SiO_2 with a flow-type reactor, but the maximum ethanol yield was less than 40 mol%.

Our research group reported Ru-Sn/TiO_2 as an effective catalyst, which converted aqueous acetic acid into ethanol with a high yield of 98 mol% (Ito et al., 2016). Because the ethanol yield increased with increasing Ru-Sn content up to 8 wt% (based on

* Corresponding author.
E-mail address: kawamoto@energy.kyoto-u.ac.jp (H. Kawamoto).

https://doi.org/10.1016/j.egyr.2020.08.007

TiO_2) but rather decreased with higher contents of 14 wt% and 20 wt%, a hydrogenation mechanism was proposed. The carbonyl group of acetic acid is coordinated to Ti, which is a Lewis acid site, at the interface between Ru-Sn and TiO_2, and the activated carbonyl carbon is more susceptible to attack by hydrogen activated on Ru-Sn (Ito et al., 2016; Kawamoto et al., 2016).

Ru is a precious metal, but inexpensive catalysts are preferable for hydrogenation of aqueous acetic acid. Olcay et al. (2010) compared the relative catalytic activities of seven transition metals for the hydrogenation of aqueous acetic acid and reported that the catalytic activities were higher in the following order: Ru>Rh≒Pt>Pd≒Ir>Ni>Cu. According to this order, Ni is a non-precious metal candidate that can be applied to TiO_2-based catalysts instead of Ru. However, Ni/TiO_2 catalyst has not been investigated for catalytic hydrogenation of aqueous acetic acid.

Therefore, this research investigated various Ni- and Ni-Sn catalysts supported on TiO_2 for bioethanol production. The properties compared to the previous catalyst, Ru-Sn/TiO_2, were also described.

2. Experimental methods

2.1. Materials

Titanium isopropoxide (>95% purity), nickel(II) chloride hexahydrate ($NiCl_2 \cdot 6H_2O$, >98%), tin(II) chloride dihydrate ($SnCl_2 \cdot 2H_2O$, >97%), sodium hydroxide (NaOH, >97%), 2-propanol (>99%) and hydrochloric acid (HCl, 6 mol/L) were used for the catalyst preparation steps. All of the reagents were purchased from Nacalai Tesque, Inc., Kyoto, Japan.

2.2. Catalyst preparation

For catalyst preparation, our preliminary study revealed that the sol–gel sedimentation method could achieve a high dispersion of Ni and better catalytic activity than the sol–gel method. Details are provided as Supporting Information, (Table S1). Therefore, Ni/TiO_2 and Ni-Sn/TiO_2 catalysts were prepared by the sol–gel sedimentation method.

Designated amounts of $NiCl_2 \cdot 6H_2O$, $SnCl_2 \cdot 2H_2O$, or both were added to water (100 mL, 60 °C) as Ni and Sn precursors, respectively. Using a magnetic stirrer, a mixture of 2-propanol (20.0 mL) and titanium isopropoxide (37.2 mL) was added dropwise. After waiting for 0.5 h, precipitates of TiO_2 were produced by hydrolysis of titanium isopropoxide. Then, aqueous NaOH solution (100 mL, with sufficient concentration for neutralizing metal chlorides) was added and stirred for 0.5 h. During this period, $NiCl_2$ and $SnCl_2$ were converted to $Ni(OH)_2$ and $Sn(OH)_2$, respectively. The reaction mixture was allowed to stand for 12 h. Because $Ni(OH)_2$ and $Sn(OH)_2$ have low solubility to water, they were deposited on the TiO_2 surface to form composites. The obtained precipitates were washed with water five times and then oven-dried at 105 °C for 12 h.

The oven-dried precipitates were placed in a quartz combustion boat in a glass tube and calcined at 450 °C for 1 h under an airflow, and then reduced under an H_2 flow (100 mL/min) at 400 °C for 5 h. The Ni/TiO_2 and Ni-Sn/TiO_2 catalysts were thus obtained.

2.3. Catalyst characterization

The obtained catalysts were analyzed by X-ray diffraction (XRD; RINT 2000 V, Rigaku Corp., Tokyo, Japan), and the XRD patterns were identified by comparison to a database (AtomWork, National Institute for Materials Science, Ibaraki, Japan). The catalyst surface, dispersion of metals, and particle size were observed by scanning electron microscope (SEM; SU6600, Hitachi High-Technologies Corp., Tokyo, Japan) with an energy dispersive X-ray spectroscope (EDS; XFlash 5010, Bruker Corp., MA, USA), and field emission transmission electron microscope (FE-TEM; JEM-2100F, JEOL Ltd., Tokyo, Japan) with EDS (JED-2300T, JEOL Ltd.). The states of metals on catalyst surface were determined by X-ray photoelectron spectroscopy (XPS; JPS-9030, JEOL Ltd., Tokyo, Japan).

The reducibility of non-reduced Ni, Sn, Ni-Sn, and Ni-Sn/TiO_2 samples were investigated by temperature-programmed reduction (TPR; AutoChemII 2920, Micromeritics Corp., GA, USA). The sample was pretreated at 200 °C for 0.3 h under He (50 mL/min) atmosphere. The reduction was carried out from 80 to 1000 °C (10 °C/min) under 5 vol% H_2 in Ar with a flow rate of 50 mL/min.

Lewis acid points of the catalysts were determined with infrared spectroscopy (IR; IRTracer-100, Shimazu Corp., Kyoto, Japan) by using pyridine as a probe molecule (Kikuchi, 2013). Each catalyst sample was filled in a cup of a diffuse reflectance measuring device, and heated to 120 °C under vacuum pressure as a pretreatment, and then gradually cooled to 40 °C to measure the background. After that, pyridine in a 30-mL glass container was introduced, and the IR spectrum was measured.

2.4. Hydrogenation of aqueous acetic acid to ethanol

Hydrogenation was conducted in a 100-mL batch-type reactor made of Hastelloy C-278 (Model 4560, Parr Instrument Company, IL, USA). The prepared Ni/TiO_2 or Ni-Sn/TiO_2 catalyst (1.20 g) was placed in the reactor with water (20 mL), and activated with stirring at 120 °C under 2 MPa of H_2 (99.9%, Imamura Sanso KK., Otsu, Japan) for 1 h. After cooling and opening the reactor, acetic acid and water were added, adjusting the amount and concentration of aqueous acetic acid solution to be 30 mL and 10 g/L, respectively.

After sealing the reactor again, the inside of the reactor was purged and pressurized to approximately 5.4–6.6 MPa with H_2. This pressure range of H_2 provides sufficient excess and approximately 30–37 times of the required amount for hydrogenation; 1 mole of acetic acid requires 2 moles of H_2. Hydrogenation of the aqueous acetic acid was then performed with stirring at the temperature between 170–280 °C for 3–12 h. When the temperature of the reactor was increased, the inside pressure increased. Therefore, the initial H_2 pressure mentioned above was adjusted to let the pressure be about 10 MPa during the reaction.

After hydrogenation, the reactor was cooled and the reaction mixture was collected. The products in the reaction mixture were analyzed by high-performance liquid chromatography (HPLC; LC20 system, Shimadzu Corp., Kyoto, Japan) under the following conditions: column, Aminex HPX-87H (300 × 7.8 mm, Bio-Rad Laboratories, Inc., CA, USA); eluent, 5 mM sulfuric acid in water; flow-rate, 0.6 mL/min; column temperature, 45 °C; detector, refractive index detector (RID-20A, Shimadzu Corp.).

3. Results and discussion

3.1. Influence of Sn loading on the catalytic activity of Ni/TiO_2

The catalytic activity of 4wt%Ni/TiO_2 (metal basis on TiO_2) was investigated under the conditions of 220 °C/10 MPa, but the ethanol yield was only 5 mol% (Table S1). However, when the 4wt%Ni-4wt%Sn/TiO_2 catalyst was used, the ethanol yield increased significantly to 87 mol% under the same reaction conditions (Table S1). These results indicate that adding Sn promoted the catalytic activity of Ni/TiO_2 for hydrogenation of aqueous acetic acid.

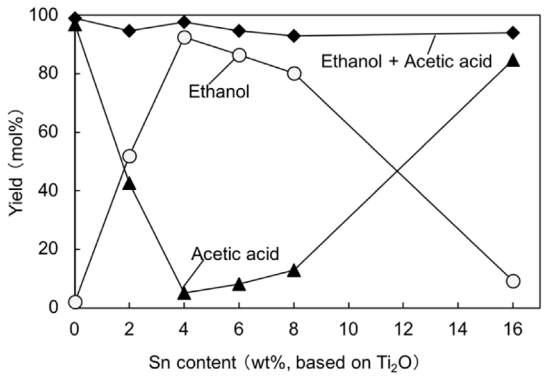

Fig. 1. The effect of Sn content on ethanol yield by hydrogenation of aqueous acetic acid (10 g/L) with 4wt%Ni-Xwt%Sn/TiO_2, (200 °C/12 h/H_2/10 MPa).

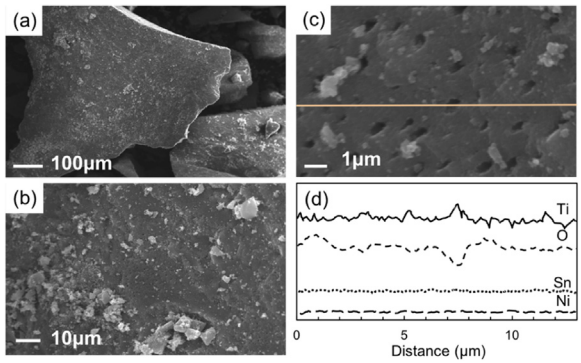

Fig. 2. SEM images of 4wt%Ni-4wt%Sn/TiO_2 at various scales (a–c) and a line mapping of elements on (c), as shown in (d).

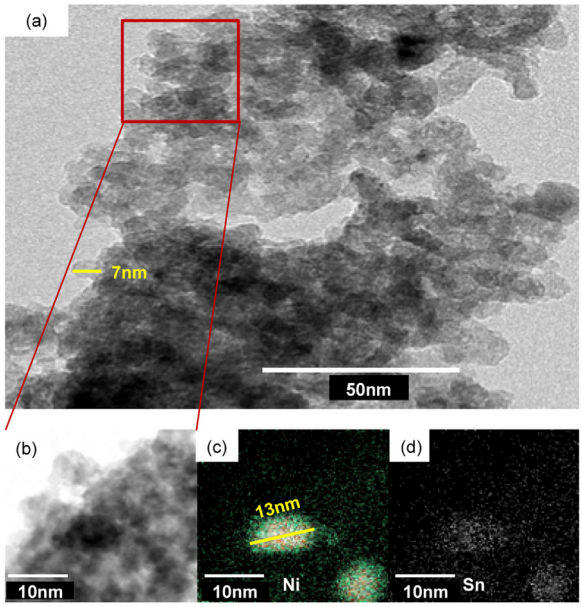

Fig. 3. Alloy dispersion on 4wt%Ni-4wt%Sn/TiO_2; (a) FE-TEM image, (b) enlarged FE-TEM image with (c) Ni and (d) Sn mappings.

The influence of Sn addition was fairly different from that observed for 4wt%Ru/TiO_2 (Ito et al., 2016). The Ru catalyst itself had a quite high catalytic activity for hydrogenation of aqueous acetic acid into ethanol, but the ethanol yield was limited due to the gas formation as a side reaction. The addition of Sn to Ru was dramatically suppressed the gas formation, improving the selectivity of ethanol production. In contrast, 4wt%Ni/TiO_2 exhibited almost no catalytic activity, and the addition of Sn was necessary for the conversion of aqueous acetic acid.

To determine the optimum Sn content, the Sn content was varied from 0 to 16 wt% with a fixed Ni content of 4 wt%. The catalytic activities of the prepared catalysts were investigated under the conditions of 200 °C/10 MPa for 12 h, and the results are shown in Fig. 1. When the Sn content increased to 2 wt% and 4 wt%, the ethanol yield was sharply improved to 51.8 mol% and 92.5 mol%, respectively. However, as the Sn content further increased to 6 wt% and 8 wt%, the ethanol yield decreased. When the Sn content reached 16 wt%, the ethanol yield drastically decreased to 9.2 mol%. Further, while increasing the Sn content from 2 wt% to 16 wt%, the color of the catalyst (as-prepared) changed from black to yellow. The reason for this color change is discussed in Section 3.3. These results indicate that approximately equal weights of Ni and Sn are optimal for the synthesis of highly efficient catalysts for hydrogenation of acetic acid.

As for the selectivity of hydrogenation, although the ethanol yield varied with the Sn content, the total yield of ethanol and acetic acid was almost 100 mol%. Therefore, the selectivity of Ni-Sn/TiO_2 for hydrogenation was found to be high, and there was no undesirable side reaction, such as gasification, under the given reaction conditions.

3.2. Characterization of Ni-Sn/TiO_2 catalyst by SEM and TEM

SEM images of a fresh 4wt%Ni-4wt%Sn/TiO_2 catalyst are shown in Fig. 2 along with a line mapping of elements by EDS. In the SEM images, lumps of the catalyst of several hundred micrometers were observed, but the detailed structures could not be observed even when the scale was enlarged. In the line mapping curves, which represent the amount of each element, no apparent change was observed for Ni and Sn, indicating that the Ni-Sn alloys were evenly dispersed on TiO_2 at the nanoscale. The formation of Ni_3Sn_2 on the catalyst surface was confirmed by XRD analysis, as described later, which reasonably explains the SEM-EDS results.

The fresh 4wt%Ni-4wt%Sn/TiO_2 catalyst was observed by FE-TEM to understand the details of alloy dispersion, and the results are shown in Fig. 3. The average sizes of the Ni-Sn alloy and TiO_2 particles were determined to be 13 ± 3 nm and 9 ± 4 nm, respectively. The reason the size of Ni-Sn alloy was larger than that of the TiO_2 support might be because the Ni-Sn alloys were loaded across several TiO_2 particles.

3.3. Optimum ratio of Ni and Sn

To discuss the reason why the optimal ratio of Ni and Sn existed, the behavior of Ni and Sn during the reduction treatment was investigated. Because Ni and Sn are the minor components of the Ni-Sn/TiO_2 catalyst, only small XRD and TPR signals were obtained. Accordingly, only Ni and Sn precursors were utilized for this study. The same sol–gel sedimentation method in Section 2.2 was conducted by using $NiCl_2$, $SnCl_2$, or both without dropping the titanium isopropoxide solution. The calcination and reduction were then carried out in the same manner at 450 °C in air for 1 h to produce metal oxides and at 400 °C in H_2 for 5 h to form metals, respectively. The prepared samples were analyzed by XRD, as shown in Fig. 4. The TPR analysis was performed for the samples before the reduction treatment and the results are shown in Fig. 5.

In the XRD results, after reducing only NiO, Ni metal was detected even though the peaks of NiO remained to some extent. In the case of only SnO_2, only the peaks of SnO_2 were found even after the reduction by H_2 at 400 °C. Therefore, NiO can be easily reduced to metal, but SnO_2 is difficult to be reduced alone under the given conditions. However, when the SnO_2 was reduced in

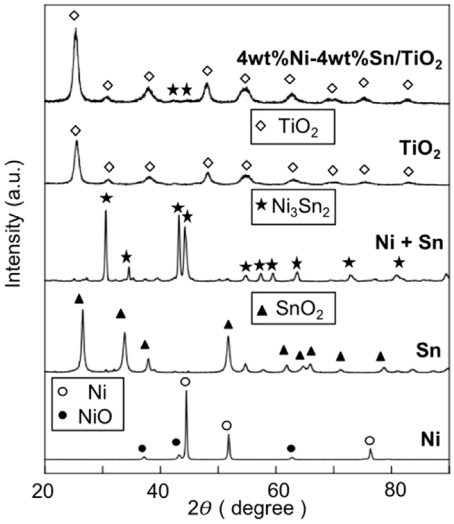

Fig. 4. Results of the reduction treatment with H_2 at 400 °C for NiO, SnO_2, or both (Ni:Sn = 1:1, w/w) analyzed by XRD.

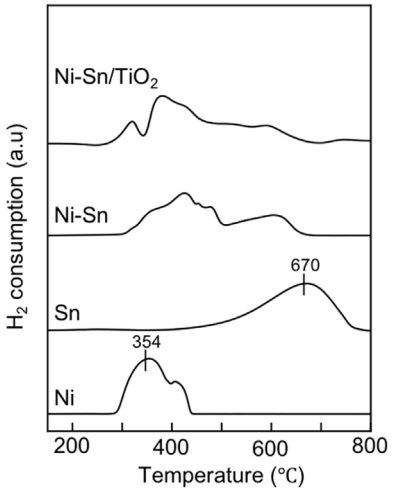

Fig. 5. TPR profiles of NiO, SnO_2, mixture of both (Ni:Sn = 1:1, w/w) and non-reduced 4wt%Ni-4wt%Sn/TiO_2.

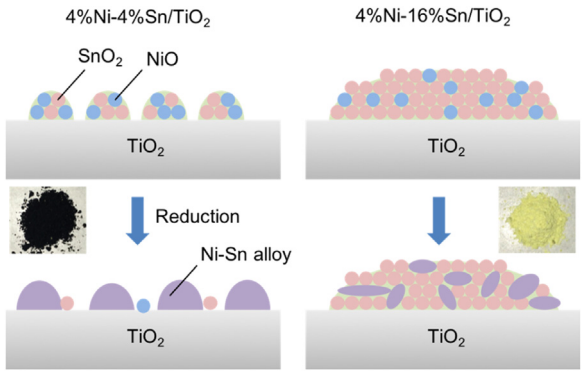

Fig. 6. The effect of Ni/Sn ratios on the alloy formation.

the presence of NiO, the peaks of Ni_3Sn_2 alloy appeared; similar results are reported in the literature (Rodiansono et al., 2012).

In the TPR profiles in Fig. 5, the reduction of NiO occurred at around 300 to 430 °C, whereas the SnO_2 required higher temperatures of around 600 to 750 °C for the reduction to Sn-metal. Similar results have been reported by others (Hengne et al., 2018; Shen et al., 2019). The reduction of the mixture of NiO and SnO_2 started at around 300 °C, like NiO only, but new peaks appeared at around 430 to 500 °C. The Sn reduction seems to conclude at around 650 °C, which is lower than in the case of SnO_2 only. These new peaks and earlier reduction of SnO_2 indicate Ni-Sn alloy formation. Wang et al. (2016) and Liu et al. (2019) have reported similar behavior in TPR profiles of Ni-Sn/SiO_2. The TPR profile of 4wt%Ni- 4wt%Sn/TiO_2 also showed similar reducibility as the mixture of NiO and SnO_2.

These results suggest that in the metal formation of the Ni-Sn/TiO_2 catalyst, Ni is first reduced by H_2, and then the metal Ni reduces adjacent SnO_2 to form the Ni_3Sn_2 alloy. Based on this assumption, the effect of the Ni/Sn ratio on the alloy formation process can be proposed as in Fig. 6. When there is an optimal Ni/Sn ratio (left figure), most of SnO_2 can be reduced to Ni-Sn alloy and it is evenly dispersed on the TiO_2 surface. However, if Sn is added excessively (right figure), only a part of SnO_2 is reduced to Ni-Sn alloy and most of the alloy is buried in the remaining SnO_2. Via this mechanism, we can also explain why the color of the catalyst changed from black to yellow when the Sn content was increased. As explained in Fig. 1, the catalytic activity was the highest for the Ni:Sn ratio of 1:1 (w/w). Because the atomic weights of Ni and Sn are 58.7 and 118.7, respectively, the weight ratio of Ni:Sn = 1:1 corresponds approximately to a molar ratio of Ni:Sn = 2:1, which is roughly similar to the stoichiometric ratio of Ni_3Sn_2 alloy. This might be the reason why the catalytic activity of the Ni-Sn/TiO_2 catalyst was high when the amounts of Ni and Sn were 4 wt% each.

3.4. Influence of reaction temperature and metal content

The aqueous acetic acid solution could be effectively converted to ethanol by using the 4wt%Ni-4wt%Sn/TiO_2 catalyst. To optimize the reaction temperature, the hydrogenation activity was evaluated in the temperature range of 180 to 280 °C at 10 MPa for 12 h, and the results are shown in Fig. 7. Ethanol reached a maximum yield of 92.5 mol% at 200 °C, and the yield tended to decrease gradually when the reaction temperature was further raised. At temperatures higher than 200 °C, the total yield of ethanol and acetic acid decreased, thus indicating that side reactions, such as gasification, proceeded. However, in the case of Ru-Sn/TiO_2 catalyst (Ito et al., 2016), gasification proceeds even at around 175 °C, so the Ni-Sn/TiO_2 catalyst is considered to have higher resistance against side reactions. Based on these results, 200 °C is the optimum temperature for hydrogenation of acetic acid with the Ni-Sn/TiO_2 catalyst. At 200 °C, the ethanol yield increased from 49 mol% to 71 mol% and 93 mol% by prolonging the reaction time from 3 h to 6 h and 12 h, respectively.

For further improved catalytic activity, the content of Ni and Sn to TiO_2 was increased up to 24 wt% each with a constant Ni:Sn ratio of 1:1 (w/w) and hydrogenation activities were investigated under 10 MPa at 200 °C for 3 h, as shown in Fig. 8. The ethanol yield was improved from approximately 50 mol% to 85 mol% when the metal contents of Ni and Sn were increased from 4 wt% to 16 wt%. However, when the metal content was further increased to 24 wt%, the ethanol yield was reduced to 57 mol%. These results indicate that there is an appropriate value for the amount of catalyst metal and that an excessive amount leads to a decrease in catalyst activity. The balance of Ni-Sn and TiO_2 may be important because increasing the amount of Ni-Sn alloy improves hydrogen activation but reduces Lewis acid sites by covering the TiO_2 surface. In this research, the 16wt%Ni-16wt%Sn/TiO_2 catalyst showed the highest catalytic activity of the systems studied.

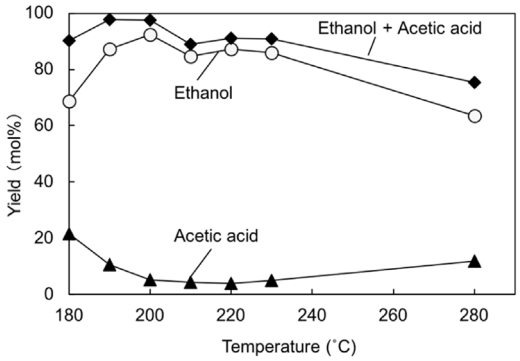

Fig. 7. Influence of temperature on hydrogenation activity of 4wt%Ni-4wt%Sn/TiO_2, reaction time (12 h).

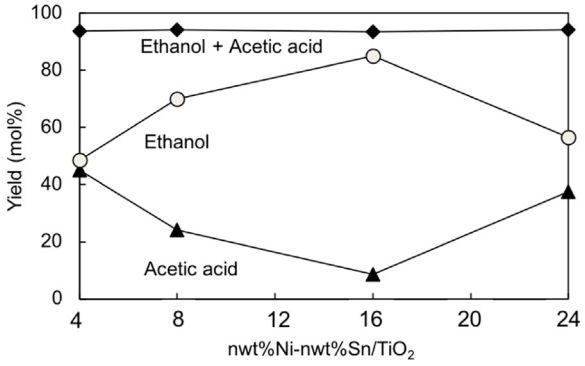

Fig. 8. The effect of metal loading amount on activity of aqueous acetic acid hydrogenation. (10 g/L AcOH, 10 MPa/3 h/200 °C).

3.5. Catalytic mechanism and comparison with Ru-Sn/TiO_2

IR analysis is useful for evaluating the acidic properties of a solid surface using pyridine as a probe molecule (Kikuchi, 2013). The acidic property of the 4wt%Ni-4wt%Sn/TiO_2 catalyst was investigated by the IR method and compared with those of TiO_2, SnO_2 and Ni_3Sn_2, and the results are shown in Fig. 9. The Lewis acid sites were detected at around 1440 cm^{-1} in TiO_2 and 4wt%Ni-4wt%Sn/TiO_2 catalyst, but there was no absorbed pyridine signal in the Ni_3Sn_2 alloy and SnO_2. This indicates that the Lewis acid sites in the catalyst were provided by TiO_2, and Ni_3Sn_2 alloys were mainly employed for activating hydrogen, although Lewis acidity of SnO_2 was used to explain the activity of Sn containing catalysts (Khder, 2008; Khder et al., 2008; Khder and Ahmed, 2009; Liu et al., 2015).

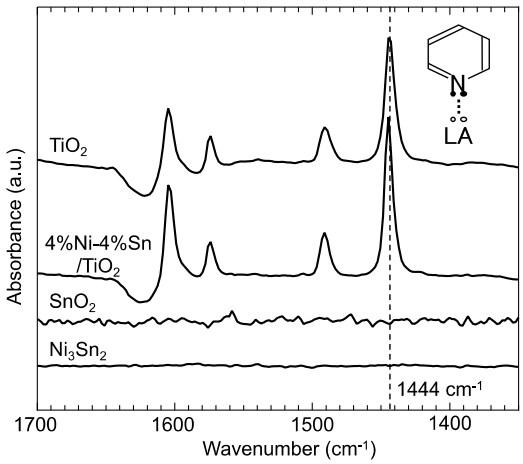

Fig. 9. Lewis acid point in the catalyst measured by IR.

The electronic states of Ni and Sn of 4wt%Ni-4wt%Sn/TiO_2 catalyst were evaluated by XPS (Fig. 10). A peak around 855 eV was assigned to Ni $2p_{3/2}$ (Li et al., 2017; Wei et al., 2004), and it contained two signals of Ni^0 with the peak at 852.1 eV (Hengne et al., 2018) and Ni^{2+} at 854.7 eV (Li et al., 2016) in Fig. 10(a). A Sn $3d_{5/2}$ signal around 486 eV, Fig. 10(b), was able to be separated into three components of Sn^0, Sn^{2+}, and Sn^{4+} with the peaks at 485, 486.2, and 487.1 eV, respectively (Li et al.,

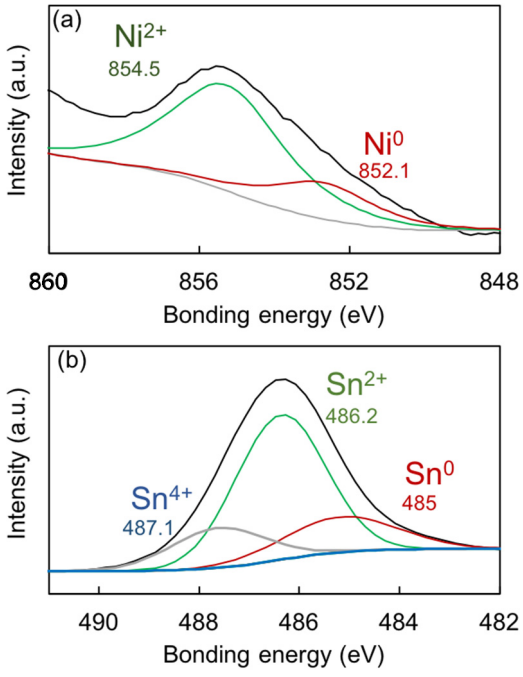

Fig. 10. Ni 2p spectra (a) and Sn 3d (b) spectra of fresh 4wt%Ni-4wt%Sn/TO_2 catalyst.

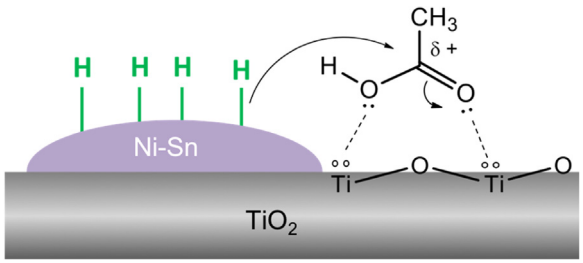

Fig. 11. Postulated role of TiO_2 and Ni-Sn alloy for the formation of ethanol from acetic acid.

2011; Quackenbush et al., 2013; Hanyš et al., 2006). These results indicate that NiO, SnO and SnO_2 remained on the catalyst surface. Nevertheless, the analysis in Fig. 9 indicates that the TiO_2 support acted as the Lewis acid site, activating acetic acid in catalytic hydrogenation in aqueous solution.

These results provide experimental support for the catalytic mechanism of Ni-Sn/TiO_2 to convert aqueous acetic acid into ethanol (Fig. 11), which was originally proposed for Ru-Sn/TiO_2 in our previous paper (Ito et al., 2016) but enough evidence has not been presented. A lone pair of carbonyl group of acetic acid coordinates to Ti of TiO_2 as a Lewis acid, activating the acetic acid molecule by increasing the δ^+ character of carbonyl carbon. This makes the nucleophilic addition of hydrogen anion that is activated on Ni-Sn alloy easier. With this mechanism, hydrogenation of acetic acid occurs at the interface between Ni-Sn and TiO_2. The hydrogenation reactivity that rather decreased by using a large excess amount of Ni-Sn alloy (24 wt%, based on TiO_2, Fig. 8) supports this mechanism.

Both Ru-Sn/TiO_2 and Ni-Sn/TiO_2 catalysts exhibited high catalytic activity for hydrogenation of aqueous acetic acid into ethanol. The yield of ethanol with Ni-Sn/TiO_2 catalyst was 93 mol% under conditions of 200 °C/ 10 MPa/ 12 h, corresponding to that (98 mol%) with Ru-Sn/TiO_2 under similar conditions of 170 °C/ 15 MPa/ 12 h (Ito et al., 2016). However, the role of Sn is quite different for these catalysts. The catalytic activity decreased by changing Ru metal to Ru-Sn alloy, but the selectivity of ethanol formation increased by suppressing gasification as a side reaction more significantly. On the other hand, the catalytic activity of Ni catalyst was dramatically enhanced by using Ni-Sn alloy, probably due to the more efficient hydrogen activation occurring on Ni-Sn alloy than Ni metal.

4. Conclusions

The Ni/TiO_2 and Ni-Sn/TiO_2 catalysts were investigated for hydrogenation of aqueous acetic acid to ethanol, relating to the bioethanol production from lignocellulosics. Catalytic activities of Ni/TiO_2 catalysts were low but dramatically increased by the addition of Sn, and the ethanol yield reached 93 mol% with 4wt%Ni-4wt%Sn/TiO_2. The optimum ratio of Ni:Sn was about 1:1 (w/w) for high catalytic activity due to the alloy (Ni_3Sn_2) formation, where NiO is first reduced by H_2 into Ni metal, and then the Ni metal reduces the adjacent SnO_2 to form Ni-Sn alloy. Thus, the use of an excessive amount of Sn lowered the catalytic activity. The TiO_2 support was suggested to be the Lewis acid site of the catalyst. Based on the present results, the catalytic hydrogenation mechanism of Ni-Sn/TiO_2 was proposed. A lone pair of carbonyl group of acetic acid coordinates to TiO_2, resulting in enhancement of the attack of hydrogen anions activated on the neighboring Ni-Sn alloys, and thus the promotion of the hydrogenation activity.

CRediT authorship contribution statement

Yuanyuan Zhao: Investigation, Visualization, Methodology, Data curation, Writing - original draft. **Takayuki Nishida:** Investigation, Formal analysis. **Eiji Minami:** Supervision, Writing - review & editing. **Shiro Saka:** Supervision, Conceptualization. **Haruo Kawamoto:** Supervision, Conceptualization, Writing - review & editing.

Declaration of competing interest

The authors declare that they have no known competing financial interests or personal relationships that could have appeared to influence the work reported in this paper.

Acknowledgments

This work was supported by the Japan Science and Technology Agency (JST) under the Advanced Low Carbon Technology Research and Development Program (ALCA). We thank Iain Mackie, Ph.D., from Edanz Group (www.edanzediting.com/ac) for editing a draft of this manuscript.

Appendix A. Supplementary data

Supplementary material related to this article can be found online at https://doi.org/10.1016/j.egyr.2020.08.007.

References

Adkins, H., Folkers, K., 1931. The catalytic hydrogenation of esters to alcohols. J. Am. Chem. Soc. 53, 1095–1097. http://dx.doi.org/10.1021/ja01354a042.

Adkins, H., Wojcik, B., Covert, W.L., 1933. The catalytic hydrogenation of esters to alcohols. III. J. Am. Chem. Soc. 55, 1669–1676. http://dx.doi.org/10.1021/ja01331a060.

Ajanovic, A., 2011. Biofuels versus food production: does biofuels production increase food prices? Energy 36, 2070–2076. http://dx.doi.org/10.1016/j.energy.2010.05.019.

Biello, D., 2011. The false promise of biofuels. Sci. Am. 305, 58–65. http://dx.doi.org/10.1038/scientificamerican0811-58.

Chien, I.L., Zeng, K.L., Chao, H.Y., Liu, J.H., 2004. Design and control of acetic acid dehydration system via heterogeneous azeotropic distillation. Chem. Eng. Sci. 59, 4547–4567. http://dx.doi.org/10.1016/j.ces.2004.06.041.

Cleveland, C.J., Costanza, R., Hall, C.A.S., Kaufmann, R., 1984. Energy and the U.S. economy: a biophysical perspective. Science 225, 890–897. http://dx.doi.org/10.1126/science.225.4665.890.

Elliott, D.C., Hart, T.R., 2009. Catalytic hydroprocessing of chemical models for bio-oil. Energy Fuel 23, 631–637. http://dx.doi.org/10.1021/ef8007773.

Folkers, K., Adkins, H., 1932. The catalytic hydrogenation of esters to alcohols. II. J. Am. Chem. Soc. 54, 1145–1154. http://dx.doi.org/10.1021/ja01342a043.

Hanyš, P., Janeček, P., Matolín, V., Korotcenkov, G., Nehasil, V., 2006. XPS and TPD study of Rh/SnO_2 system - reversible process of substrate oxidation and reduction. Surf. Sci. 600, 4233–4238. http://dx.doi.org/10.1016/j.susc.2006.01.150.

Hengne, A.M., Samal, A.K., Enakonda, L.R., Harb, M., Gevers, L.E., Anjum, D.H., Hedhili, M.N., Saih, Y., Huang, K.W., Basset, J.M., 2018. Ni-Sn-supported ZrO_2 catalysts modified by indium for selective CO_2 hydrogenation to methanol. ACS Omega 3, 3688–3701. http://dx.doi.org/10.1021/acsomega.8b00211.

Ito, Y., Kawamoto, H., Saka, S., 2016. Efficient and selective hydrogenation of aqueous acetic acid on Ru-Sn/TiO_2 for bioethanol production from lignocellulosics. Fuel 178, 118–123. http://dx.doi.org/10.1016/j.fuel.2016.03.043.

Kawamoto, H., Fujii, T., Ito, Y., Saka, S., 2016. Effects of different solvents on hydrogenation of acetic acid over Pt/TiO_2 for bioethanol production. J. Jpn. Inst. Energy 95, 162–166. http://dx.doi.org/10.3775/jie.95.162.

Khder, A.E.R.S., 2008. Preparation, characterization and catalytic activity of tin oxide-supported 12-tungstophosphoric acid as a solid catalyst. Appl. Catal. A Gen. 343, 109–116. http://dx.doi.org/10.1016/j.apcata.2008.03.027.

Khder, A.S., Ahmed, A.I., 2009. Selective nitration of phenol over nanosized tungsten oxide supported on sulfated SnO_2 as a solid acid catalyst. Appl. Catal. A Gen. 354, 153–160. http://dx.doi.org/10.1016/j.apcata.2008.11.030.

Khder, A.S., El-Sharkawy, E.A., El-Hakam, S.A., Ahmed, A.I., 2008. Surface characterization and catalytic activity of sulfated tin oxide catalyst. Catal. Commun. 9, 769–777. http://dx.doi.org/10.1016/j.catcom.2007.08.022.

Kikuchi, E., 2013. New Catalytic Chemistry. Sankyo Shuppan Co., Ltd., Tokyo, Japan, ISBN: 978-4782706886, (in Japanese).

Lei, Z., Li, C., Li, Y., Chen, B., 2004. Separation of acetic acid and water by complex extractive distillation. Sep. Purif. Technol. 36, 131–138. http://dx.doi.org/10.1016/S1383-5866(03)00208-9.

Li, B., Li, C., Cai, J.C., Zhao, J., 2016. In situ nano-coating on $Li_{1.2}Mn_{0.52}Ni_{0.13}Co_{0.13}O_2$ with a layered@spinel@coating layer heterostructure for lithium-ion batteries. J. Mater. Chem. A 4, 14884. http://dx.doi.org/10.1039/c6ta90179d, (erratum).

Li, J.T., Świątowska, J., Maurice, V., Seyeux, A., Huang, L., Sun, S.G., Marcus, P., 2011. XPS and ToF-SIMS study of electrode processes on Sn-Ni alloy anodes for Li-ion batteries. J. Phys. Chem. C 115, 7012–7018. http://dx.doi.org/10.1021/jp201232n.

Li, X., Xin, M., Guo, S., Cai, T., Du, D., Xing, W., Zhao, L., Guo, W., Xue, Q., Yan, Z., 2017. Insight of synergistic effect of different active metal ions in layered double hydroxides on their electrochemical behaviors. Electrochim. Acta 253, 302–310. http://dx.doi.org/10.1016/j.electacta.2017.09.075.

Liu, X., Liu, X., Xu, G., Zhang, Y., Wang, C., Lu, Q., Ma, L., 2019. Highly efficient catalytic conversion of cellulose into acetol over Ni-Sn supported on nanosilica and the mechanism study. Green Chem. 21, 5647–5656. http://dx.doi.org/10.1039/c9gc02449b.

Liu, Q., Yang, F., Liu, Z., Li, G., 2015. Preparation of SnO_2-Co_3O_4/C biochar catalyst as a Lewis acid for corncob hydrolysis into furfural in water medium. J. Ind. Eng. Chem. 26, 46–54. http://dx.doi.org/10.1016/j.jiec.2014.11.041.

Nakamura, Y., Miyafuji, H., Kawamoto, H., Saka, S., 2011. Acetic acid fermentability with *clostridium thermoaceticum* and *clostridium thermocellum* of standard compounds found in beech wood as produced in hot-compressed water. J. Wood Sci. 57, 331–337. http://dx.doi.org/10.1007/s10086-010-1169-3.

Olcay, H., Xu, L., Xu, Y., Huber, G.W., 2010. Aqueous-phase hydrogenation of acetic acid over transition metal catalysts. ChemCatChem 2, 1420–1424. http://dx.doi.org/10.1002/cctc.201000134.

Osei, G., Arthur, R., Afrane, G., Agyemang, E.O., 2013. Potential feedstocks for bioethanol production as a substitute for gasoline in ghana. Renew. Energy 55, 12–17. http://dx.doi.org/10.1016/j.renene.2012.12.012.

Pimentel, D., Marklein, A., Toth, M.A., Karpoff, M., Paul, G.S., McCormack, R., Kyriazis, J., Krueger, T., 2008. Biofuel impacts on world food supply: use of fossil fuel, land and water resources. Energies 1, 41–78. http://dx.doi.org/10.3390/en1010041.

Quackenbush, N.F., Allen, J.P., Scanlon, D.O., Sallis, S., Hewlett, J.A., Nandur, A.S., Chen, B., Smith, K.E., Weiland, C., Fischer, D.A., Woicik, J.C., White, B.E., Watson, G.W., Piper, L.F.J., 2013. Origin of the bipolar doping behavior of SnO from X-ray spectroscopy and density functional theory. Chem. Mater. 25, 3114–3123. http://dx.doi.org/10.1021/cm401343a.

Rabemanolontsoa, H., Yoshimizu, K., Saka, S., 2016. High conversion efficiency of Japanese cedar hydrolyzates into acetic acid by co-culture of *clostridium thermoaceticum* and *clostridium thermocellum*. J. Chem. Technol. Biotechnol. 91, 1040–1047. http://dx.doi.org/10.1002/jctb.4679.

Rachmady, W., Vannice, M.A., 2000. Acetic acid hydrogenation over supported platinum catalysts. J. Catal. 192, 322–334. http://dx.doi.org/10.1006/jcat.2000.2863.

Rodiansono, Khairi, S., Hara, T., Ichikuni, N., Shimazu, S., 2012. Highly efficient and selective hydrogenation of unsaturated carbonyl compounds using Ni-Sn alloy catalysts. Catal. Sci. Technol. 2, 2139–2145. http://dx.doi.org/10.1039/c2cy20216f.

Rodríguez, L.A., Toro, M.E., Vazquez, F., Correa-Daneri, M.L., Gouiric, S.C., Vallejo, M.D., 2010. Bioethanol production from grape and sugar beet pomaces by solid-state fermentation. Int. J. Hydrog. Energy 35, 5914–5917. http://dx.doi.org/10.1016/j.ijhydene.2009.12.112.

Saka, S., Rabemanolontsoa, H., Minami, E., Kawamoto, H., 2019. Advanced ethanol production with acetic acid fermentation from lignocellulosics. J. Jpn. Petrol. Inst. 62, 199–204. http://dx.doi.org/10.1627/jpi.62.199.

Shen, J., Feng, X., Liu, R., Xu, X., Rao, C., Liu, J., Fang, X., Tan, C., Xie, Y., Wang, X., 2019. Tuning SnO_2 surface with CuO for soot particulate combustion: the effect of monolayer dispersion capacity on reaction performance. Chinese J. Catal. 40, 905–916. http://dx.doi.org/10.1016/S1872-2067(19)63354-1.

Voeste, T., Buchold, H., 1984. Production of fatty alcohols from fatty acids. J. Am. Oil Chem. Soc. 61, 350–352. http://dx.doi.org/10.1007/BF02678794.

Wan, H., Chaudhari, R.V., Subramaniam, B., 2013. Aqueous phase hydrogenation of acetic acid and its promotional effect on *p*-cresol hydrodeoxygenation. Energy Fuel 27, 487–493. http://dx.doi.org/10.1021/ef301400c.

Wang, Z., Li, G., Liu, X., Huang, Y., Wang, A., Chu, W., Wang, X., Li, N., 2014. Aqueous phase hydrogenation of acetic acid to ethanol over Ir-MoO_x/SiO_2 catalyst. Catal. Commun. 43, 38–41. http://dx.doi.org/10.1016/j.catcom.2013.09.007.

Wang, G., Wang, H., Zhang, H., Zhu, Q., Li, C., Shan, H., 2016. Highly selective and stable NiSn/SiO_2 catalyst for isobutane dehydrogenation: effects of Sn addition. ChemCatChem 8, 3137–3145. http://dx.doi.org/10.1002/cctc.201600685.

Wei, Y.J., Yan, L.Y., Wang, C.Z., Xu, X.G., Wu, F., Chen, G., 2004. Effects of Ni doping on [MnO_6] octahedron in $LiMn_2O_4$. J. Phys. Chem. B 108, 18547–18551. http://dx.doi.org/10.1021/jp0479522.